



HAL
open science

Cellulose nanofibrils prepared by twin-screw extrusion: Effect of the fiber pretreatment on the fibrillation efficiency

Khadija Trigui, Clément de Loubens, Albert Magnin, Jean-Luc Putaux, Sami Boufi

► To cite this version:

Khadija Trigui, Clément de Loubens, Albert Magnin, Jean-Luc Putaux, Sami Boufi. Cellulose nanofibrils prepared by twin-screw extrusion: Effect of the fiber pretreatment on the fibrillation efficiency. Carbohydrate Polymers, 2020, 240, pp.116342. 10.1016/j.carbpol.2020.116342 . hal-02566870v2

HAL Id: hal-02566870

<https://hal.science/hal-02566870v2>

Submitted on 10 Jun 2023

HAL is a multi-disciplinary open access archive for the deposit and dissemination of scientific research documents, whether they are published or not. The documents may come from teaching and research institutions in France or abroad, or from public or private research centers.

L'archive ouverte pluridisciplinaire **HAL**, est destinée au dépôt et à la diffusion de documents scientifiques de niveau recherche, publiés ou non, émanant des établissements d'enseignement et de recherche français ou étrangers, des laboratoires publics ou privés.

**Cellulose nanofibrils prepared by twin-screw extrusion:
Effect of the fiber pretreatment on the fibrillation efficiency**

Khadija Trigui^a, Clément De Loubens^b, Albert Magnin^b, Jean-Luc Putaux^c, Sami Boufi^a

^a University of Sfax - LMSE - Faculty of Science - BP 802 – 3018 Sfax, Tunisia

^b Univ. Grenoble Alpes, CNRS, Grenoble INP, LRP, F-38000 Grenoble, France

^c Univ. Grenoble Alpes, CNRS, CERMAV, F-38000 Grenoble, France

Published in: **Carbohydrate Polymers** 240 (2020), 116260

DOI: [10.1016/j.carbpol.2020.116342](https://doi.org/10.1016/j.carbpol.2020.116342)

Abstract

Twin-screw extrusion (TSE) is a rather recent method to produce cellulose nanofibrils (CNFs) at a high solid content under continuous feeding. Here, never-dried commercial eucalyptus pulp was used as starting material to produce CNFs by TSE after a chemical pretreatment to introduce carboxylic groups via TEMPO-mediated oxidation and carboxymethylation. Five samples with a carboxyl content ranging from 800 to 1300 $\mu\text{mol.g}^{-1}$ were produced to explore how the carboxyl content affects the aptitude of cellulose fibers to be broken down to nanoscale. The properties of the resulting CNFs in terms of nanosized fraction, morphology and rheological properties were investigated. A critical carboxyl content of 700 $\mu\text{mol.g}^{-1}$ was a prerequisite for the successful conversion of cellulose fibers into a CNF gel by TSE, regardless the pretreatment method. The degree of swelling of the fibers was put forward to account for this critical parameter.

1. Introduction

During the last decade, cellulose nanofibrils (CNFs) have gained widespread scientific and commercial interest with promising potential applications in different fields including high-volume industries such as paper and board and packaging where CNFs have demonstrated their strong strengthening effect when added in bulk as well as coating layers (Boufi et al. 2016, Lavoine et al. 2012). CNFs also find numerous uses in low-volume application as improved rheology additive of food, cosmetics, pharmaceuticals and paints, lightweight reinforced agent in composites for automotive, and sporting goods.

However, despite the progress achieved in reducing the energy cost related to the mechanical disintegration of cellulose fibers along with the diversification of production methods and of CNFs using wide range of available feedstock cellulose resources, their widespread use at the industrial scale is still limited and beyond expectation. One of the obstacles is the low consistency of CNF slurries, typically in the range of 1-3 wt%, making the transportation expense decisive in the final cost of CNFs. In addition, the high water content generates additional problems, such as excessive dilution effects when CNFs are used as additive, necessity to handle large volumes of CNF slurries and longer time for water removal.

The concentration of CNF slurries via pressure filtration or water evaporation is a possible solution to make up for transport and storage. However, this solution is highly energy consuming and capital investment is needed with additional economic impact on the final cost of CNFs. Another alternative would be the use of a high-consistency route to produce CNFs, among which twin-screw extrusion (TSE) has recently been reported as a promising method to break down cellulose fibers into CNFs with a solid content up to 20 wt% and a notably lower energy consumption (about 60 % and more) than high-pressure homogenizer or grinder widely used to produce CNFs as has been highlighted in recent papers (Rol et al. 2019, Baati, Magnin & Boufi 2017, Rolet al. 2017).

Despite the numerous advantages of TSE as a new route to produce CNFs, so far, only seven papers have been reported in the literature using the terms TSE and cellulose nanofibrils. The first work reporting the possible production of CNFs by TSE dates back 2014 when untreated never-dried refined pulp (needle-leaf bleached kraft pulp) had been extruded by TSE at a solid content ranging from 30-40 % (Ho, Zimmermann & Yano 2015). Then, in 2017, two papers were published concerning the successful disintegration of cellulose fibers into CNFs via TSE at a high solid content ranging from 10 to 17 %. In the first one, CNFs with a diameter around 5 nm and a yield in nanosized material exceeding 70 % were obtained after 30 min of

recirculation through a twin-screw minicomponenter, using a TEMPO-mediated oxidized holocellulose (Baati, Magnin & Boufi 2017). In the second paper, enzymatic pretreatment of TEMPO-oxidized eucalyptus pulp was used as starting material (Rol et al. 2017). After 7 passes through the TSE, CNFs with a width around 20-30 nm were produced with a yield in nanosized fraction in the range of 35 to 65 %, depending on the fiber pretreatment. More recently, cationized cellulose fibers with a degree of substitution (DS) around 0.3 were extruded in TSE at a solid content of 17 % to produce cationized CNFs with a width of 43 ± 20 nm estimated by AFM (Rol et al. 2019). The fraction of nanosized material evaluated by centrifugation test was found to be around 50%, meaning that TSE did not ensure the effective breakdown of cellulose fibers into nanofibrils and a high fraction of residual fibers was still present after TSE even after 7 passes. It was hypothesized that the presence of microsized fibers was due to a slipping effect of fibers into the TSE. The same approach has been used to produce phosphorylated CNFs with good flame-retardant properties. The phosphorylation was performed by treating cellulose fibers in a solution of urea and ammonium phosphate, drying at 105 °C and curing at 150 °C for 1 h to ensure the grafting of phosphate moiety on cellulose. However, the phosphorylated CNFs were composed of large microsized fiber fragments and very small nanofibers.

In our previous works (Batti, Magnin & Boufi 2017, Baati, Mabrouk, Magnin & Boufi 2018), the successful disintegration of cellulose fibers into CNFs by TSE with a high yield exceeding 80 % was demonstrated. However, it was shown that the pulping routes as well as the carboxyl content strongly affect the efficiency of the disintegration process, and only oxidized holocellulose fibers could be broken down into nanofibrils with a lateral dimension lower than 5 nm and a length within the micrometer scale. In the present work, we pursue our investigation concerning the production of CNFs at high solid content by TSE using commercial pulp instead of lab-scale pulped cellulose fibers. The main emphasis is to gain better knowledge on the effect of the chemical pretreatments (TEMPO-mediated oxidation and carboxymethylation) on the capacity of commercial bleached cellulose pulps to be disintegrated into CNFs and how the resulting CNFs are affected by the chemical pretreatment in terms of morphology, nanosized fraction, mechanical properties and rheology.

2. Experimental section

2.1 Materials

Never-dried eucalyptus pulp (NDP) kindly provided by Torraspapel with a water content of 50% was used for the production of CNFs. Sodium chlorite (NaClO_2), acetic acid (AA) 2,2,6,6-

tetramethylpiperidine-1-oxyl radical (TEMPO), sodium bromide (NaBr), isopropanol, sodium chloroacetic acid are from Sigma Aldrich and used as received. 4% sodium hypochlorite solution (NaClO) was a commercial product. Its concentration was checked by volumetric titration with sodium thiosulfate.

2.2 TEMPO-mediated oxidation

The TEMPO-mediated oxidation was carried out at pH 7 and 10, using NaClO₂ and NaClO as oxidizing agents, respectively. The oxidation protocol is as follows:

TEMPO-NaClO-,NaClO₂ (neutral oxidation)

Cellulose fibers (5 g) were dispersed in a 0.05 M sodium phosphate buffer (500 mL, pH 7) solution, containing TEMPO (200 mg). Sodium chlorite (from 2.5 to 4 g) and 20 mL NaClO solution were added to the beaker and the fiber suspension was kept under magnetic stirring during 60 °C for 12 h. Then, fibers were recovered by filtration were washed three times with deionised water and the consistency was adjusted at 10% by vacuum filtration of the fiber suspension and water addition at appropriate level. Two samples of oxidized fibers were prepared using 2.5 and 4 g of NaClO₂. They were labeled Neut-500 and Neut-800, respectively.

TEMPO-NaBr-NaClO (basic oxidation)

Cellulose fibers (4 g) were suspended in 500 mL water. TEMPO (200 mg) and NaBr (0.8 g) was added to the suspension. Then the appropriate volume of hypochlorite solution was added dropwise to the cellulose suspension at a temperature around 5 °C, kept constant throughout the oxidation reaction. The pH was maintained around 10 by the continuous addition of a 0.1 M aqueous solution of NaOH. The fibers were then recovered by filtration and copiously washed with water until neutral pH. Three samples of oxidized fibers were prepared using 300, 400 and 600 mL of hypochlorite solution. They are referred to as Bas-800, Bas-1000 and Bas-1300, respectively.

2.3 Carboxymethylation

The carboxymethylation was performed in isopropanol (IPA) as follows: 5 g of pulp was added to 300 mL IPA and the suspension was kept under magnetic stirring for 3 h after addition of 4 mL of 30 % (w/v) sodium hydroxide. The carboxymethylation reaction was started by adding sodium chloroacetic acid in 50 mL IPA to the reaction mixture placed in a water bath thermostated at 60 °C. The reaction was stopped after 6 h by cooling the mixture to room temperature and the pH of the suspension was adjusted to neutrality with acetic acid. The

mixture was then filtered and copiously washed with water until the conductivity of the suspension decreased below 200 μSm . Two samples with carboxyl content 580 and 800, referred to as Car-600 and Car-800, were prepared by adding appropriate amounts of sodium chloroacetic acid (0.65 g and 0.8 g for Carb-600 and Carb-800, respectively).

2.4 Carboxyl content

The carboxyl content of the oxidized cellulose was determined using conductometric titration, as described elsewhere (Besbes, Alila & Boufi 20xx). Briefly, around 100 mg of fibers were dispersed in 15 mL water and 5 mL 0.01 M HCl was added to bring the pH to 3 and turn all carboxyl groups in their undissociated form. Then, the suspension was titrated by NaOH solution (0.01 M) using conductivity measurement.

2.5 Water retention value (WRV)

The WRV was evaluated by centrifugation according to the method of Okubayashi et al. (Okubayashi, Griesser & Bechtold 2004). In brief, about 0.3 to 0.5 g of fiber saturated in water was centrifuged at 4000 g for 10 min, and the dry weight of the fiber was measured. The WRV was calculated from Eq. 1.

$$WRV(\%) = (W_w - W_d) / W_d * 100 \quad (\text{Eq. 1})$$

where W_w and W_d are the weight of wet and dry samples.

2.6 Preparation of CNF films

A CNF suspension with a 0.5 wt% consistency was prepared by dilution of the CNF gel and dispersed with an Ultra Turrax during 20 s at 15000 rpm. 50 mL of the suspension was then cast into a Petri dish and left in a circulated oven at 40 °C for 24 h. The CNF films were stored at 25 °C and 50 % relative humidity (R.H.) to reach moisture equilibrium absorption.

2.7 Twin-screw extrusion of fibers

Samples were processed in a laboratory scale co-rotating conical twin-screw DSM-Xplore15cc Micro-extruder, comprising a clamshell barrel with a conical twin-screw extruder, which can be operated in batch and continuous modes ensured by a recirculation channel and a control valve built into the barrel (Supplementary Material **Figure S1**). Pulps with a solid content of 10 wt% were fed in to the barrel and continuously extruded at a constant screw-speed of 200 rpm via recirculation for 20 min.

2.8 Nanosized fraction

The nanosized fraction was evaluated by centrifugation as follows: a dilute suspension with about 0.2 wt% solid content (Sc) was centrifuged at 4500 rpm for 20 min to separate the nanofibrillated material (in supernatant fraction) from the unfibrillated fibers which settled down. The nanosized fraction in % corresponds to the suspension concentration after centrifugation against the initial suspension concentration. The test was repeated at least twice and the average was reported.

2.9 Mechanical properties

Tensile tests

The mechanical properties of CNF films were investigated using an ARES rheometer (TA Instruments). Rectangular film specimen (30 mm × 5 mm) with a thickness of about 30 μm were used and a cross-head speed of 5 mm.min⁻¹ was applied. Specimens were equilibrated at 23 °C and 50% R.H. for at least 2 days to reach moisture equilibrium and five specimens were tested for each composition.

Dynamic mechanical analysis (DMA)

DMA experiments were conducted in tension mode using an ARES rheometer (TA Instruments) in tension mode. Temperature scans were run from 20 to 60 °C at a heating rate of 2 °C.min⁻¹, a frequency of 1 Hz and an amplitude of 10 μm.

2.10 Microscopy

Field-emission scanning electron microscopy (FE-SEM)

Drops of the CNF suspensions with a solid content of about 0.05 wt% were deposited on the surface of a silicon wafer and coated with a 2-3 nm-thick carbon layer by ion sputtering. Images of the film surface were recorded using an in-lens secondary electron detector in a ZEISS Gemini SEM 500 microscope equipped with a field-emission (FE) gun and operated at a low acceleration voltage (2-5 kV).

Transmission electron microscopy (TEM)

Droplets of 0.001 wt% CNF suspensions were deposited on freshly glow-discharged carbon-coated films supported by copper TEM grids. Prior to drying, a drop of 2 wt% uranyl acetate negative stain was deposited on the specimens. After 1 min, the stain in excess was blotted with filter paper and the remaining liquid film allowed to dry. The specimens were observed with a JEOL JEM 2100-Plus microscope operating at a voltage of 200 kV. The images were recorded with a Gatan Rio 16 digital camera.

Optical microscopy

Fibers were dispersed by gentle mixing in water at a concentration of about 0.5 wt% and a drop of the suspension was deposited on a glass slide covered with a slip. The optical microscopy images were taken using a Carl Zeiss Axio optical microscope in transmission mode equipped with an AxioCamMRc 5 digital camera.

2.11 Shear rheometry

The shear rheological measurements were made on DHR3 rheometer (TA Instruments). A plate-plate cell with a diameter of 25 mm was used. Its surface was rough to prevent slippage to the wall. The temperature was 25 °C maintained by Peltier heating. Dynamic mode tests under small strains were performed by measuring firstly storage modulus G' and loss modulus G'' vs. strain to determine the linear behavior domain. Then, frequency sweep at a fixed strain in the linear domain was performed.

2.12 Transmittance measurements

The optical properties of transmittance and haze of the nanopaper was obtained with a UV-Vis Lambda 35 Spectrometer (Perkin Elmer, USA), and the transmittance was measured between 700 and 400 nm. Haze is a measurement of the amount of light that is diffused or scattered when passing through a transparent material and is experimentally quantified by **Eq. 2**:

$$Haze = \frac{T_d}{T_t} \cdot 100 \quad (\text{Eq. 2})$$

Where T_d is the scattered transmitted light and T_t is the total transmitted light.

2.13 X-ray diffraction (XRD)

One millimeter-large strips of nanopaper specimens were cut and fixed with tape on 0.2 mm collimators. The films were X-rayed in a Warhus vacuum chamber using a Philips PW3830 generator operating at 30 kV and 20 mA (Ni-filtered $\text{CuK}\alpha$ radiation, $\lambda = 0.1542$ nm), during 1-h exposures. Two-dimensional diffraction patterns were recorded on Fujifilm imaging plates, read offline with a Fujifilm BAS 1800-II bioimaging analyzer. Profiles were calculated by rotational averaging of the 2D patterns. The crystallinity index (CrI) was estimated using Segal's equation (Segal, Creely, Martin & Conrad 1959):

$$CrI = \left(\frac{I_{CrS} - I_{am}}{I_{CrS}} \right) \quad (\text{Eq. 3})$$

where I_{CrS} is the intensity of the 200 peak at 22.3° and I_{am} , the intensity of the minimum between the 200 and 110 peaks at 18° .

3. Results and discussion

NDP was used as starting material to produce CNFs by TSE. This choice was motivated by the easier fibrillation aptitude of NDP compared to dried commercial pulps as will be demonstrated in the following. Without any chemical pretreatment, it was impossible to extrude NDP because of the compression of fibers at the end of the screw obstructing any possible recirculation for multiple passes. Photos showing this phenomenon are given in Supplementary Material **Figure S3**. The same effect was observed for oxidized fibers with a carboxyl content lower than 600 $\mu\text{mol.g}^{-1}$. For samples with a carboxyl content exceeding 750 $\mu\text{mol.g}^{-1}$, a successful extrusion of fibers without any clogging has been performed and a thick gel was obtained even after 10 min extrusion. Five samples of chemically treated fibers have been extruded, encompassing: three samples of fibers oxidized under basic condition having a carboxyl content of 750, 1000 and 1350 $\mu\text{mol.g}^{-1}$ (referred to as Bas-800, Bas-1000, Bas-1300), one oxidized under neutral condition with a carboxyl content around 800 $\mu\text{mol.g}^{-1}$ (referred as Neut-800) and one carboxylated fibers with a carboxyl content 820 $\mu\text{mol.g}^{-1}$ (referred to as Carb-800). The aim of the variation of the carboxyl amount was to investigate how this parameter affects the extrusion aptitude of fibers and properties of the resulting CNF dispersions. It is worth noting that under neutral condition, it was impossible to go over a carboxyl content of 800 $\mu\text{mol.g}^{-1}$, even though the amount of the oxidizing agent (NaClO_2) was doubled as well as the TEMPO catalyst. The only possibility to tailor the carboxyl content was to operate under basic condition and to adjust the concentration of NaClO to the desired level of oxidation. One possible reason accounting for this effect might be the difference in the pH during the oxidation reaction. The basic pH in the oxidation in the presence of NaClO favors the swelling of the fibers and facilitates the diffusion of reagents inside the inner micropores of the cellulose fibers while this phenomenon is less favored at pH 7. In fact, while the TEMPO-mediated oxidation as pretreatment in nanocellulose production proved popular, the oxidation under neutral pH is not widely reported in the literature, and to our knowledge only reported in three papers ([Saito et al. 2009](#), [Hirota, Tamura, Saito & Isogai 2009](#), [Besbes, Alila & Boufi 2011](#)). The leveling off of the carboxyl content was observed in two of them ([Saito et al. 2009](#), [Besbes, Alila & Boufi 2011](#)).

The properties of CNFs produced by TSE were evaluated by measuring: (i) the nanosized fraction, (ii) the mechanical performance of film of CNFs produced by casting and drying at 40 °C and (iii) the morphology of cellulose nanofibrils and CNF films. From the data collected in **Table 1**, we can note an enhancement in the extent of fibrillation yield of extruded fibers with increasing carbonyl group content. This effect was expected and was pointed out when

other disintegration methods were used such as high-pressure homogenization (Benhamou et al. 2014) or grinding (Saito, Kimura, Nishiyama & Isogai 2007). It was inferred that the presence of ionic groups within the cellulose fibers generated an osmotic pressure that favored the expansion of the fibers and reduced the interaction between cellulose fibrils by hydrogen bonding. However, with TSE, in addition to these two effects, the carboxyl groups render fibers more flexible and highly hydrated to be dragged at the end of the screw where fibers were submitted to a high compression degree.

Table 1. Different pretreated fibers and properties of CNFs and nanopapers produced from the resulting CNFs. CrI is the crystallinity index.

Treated fibers	Carboxyl content ($\mu\text{mol.g}^{-1}$)	Tensile strength [MPa]*	Tensile strength [MPa]**	Storage modulus E' (GPa)	CrI	Nanosized fraction [%]	T at 600 nm	WRV (%)
Bas-450	450	-	-	-	-	-	-	224
Bas-800	750	42 \pm 4	13 \pm 1	2.8 \pm 0.2	0.73	45 \pm 5	44	323
Bas-1000	1000	48 \pm 4	17 \pm 2	5.6 \pm 0.3	0.77	64 \pm 5	61	454
Bas-1300	1350	52 \pm 5	21 \pm 2	6.8 \pm 0.4	0.72	92 \pm 5	78	491
Neut-500	500	-	-	-	-	-	-	245
Neut-800	780	71 \pm 5	18 \pm 2	3.3 \pm 0.2	0.71	56 \pm 5	67	347
Carb-600	580	-	-	-	-	-	-	-
Carb-800	820	53 \pm 5	21 \pm 5	4.2 \pm 0.2	0.57	58 \pm 5	57	486

*nanopaper

** paper from treated fibers

The supernatant fraction of the centrifuged suspensions of extruded fibers was observed by TEM. As seen in the images of **Figure 1**, all preparations revealed entangled networks of fairly well individualized CNFs, thus validating the successful breakdown of pretreated cellulose fibers into nanofibrils. However, the Bas-800 suspension still contained a significant number of fibrils that were only locally disrupted (Fig. 1A and 1B). Additional details of the morphology of the resulting CNFs were provided by AFM observation (**Figure S2**), where indication about the lateral section of the CNFs was given from the height profile. The lateral section of Bas-800 and Bas-1000 CNFs was in the 3-9 nm range, while a lower width, around 3-4 nm, was found for Bas-1300.

Two possible reasons might explain the unsuccessful disruption of fibers by TSE with a carboxyl content lower than $700\mu\text{mol.g}^{-1}$: the first one is the insufficient density of ionic groups to overcome the cohesion of cellulose fibrils through hydrogen bonding. The second one might be related to the morphology of the treated cellulose fibers. To access this effect, optical microscopy observation of the neat and treated cellulose fibers was performed (**Figure 2**). Neat

NDP fibers are composed of different cell elements including long fibers, about 15 μm -wide vessel elements, collenchyma lamellar elongated cells and tracheids.

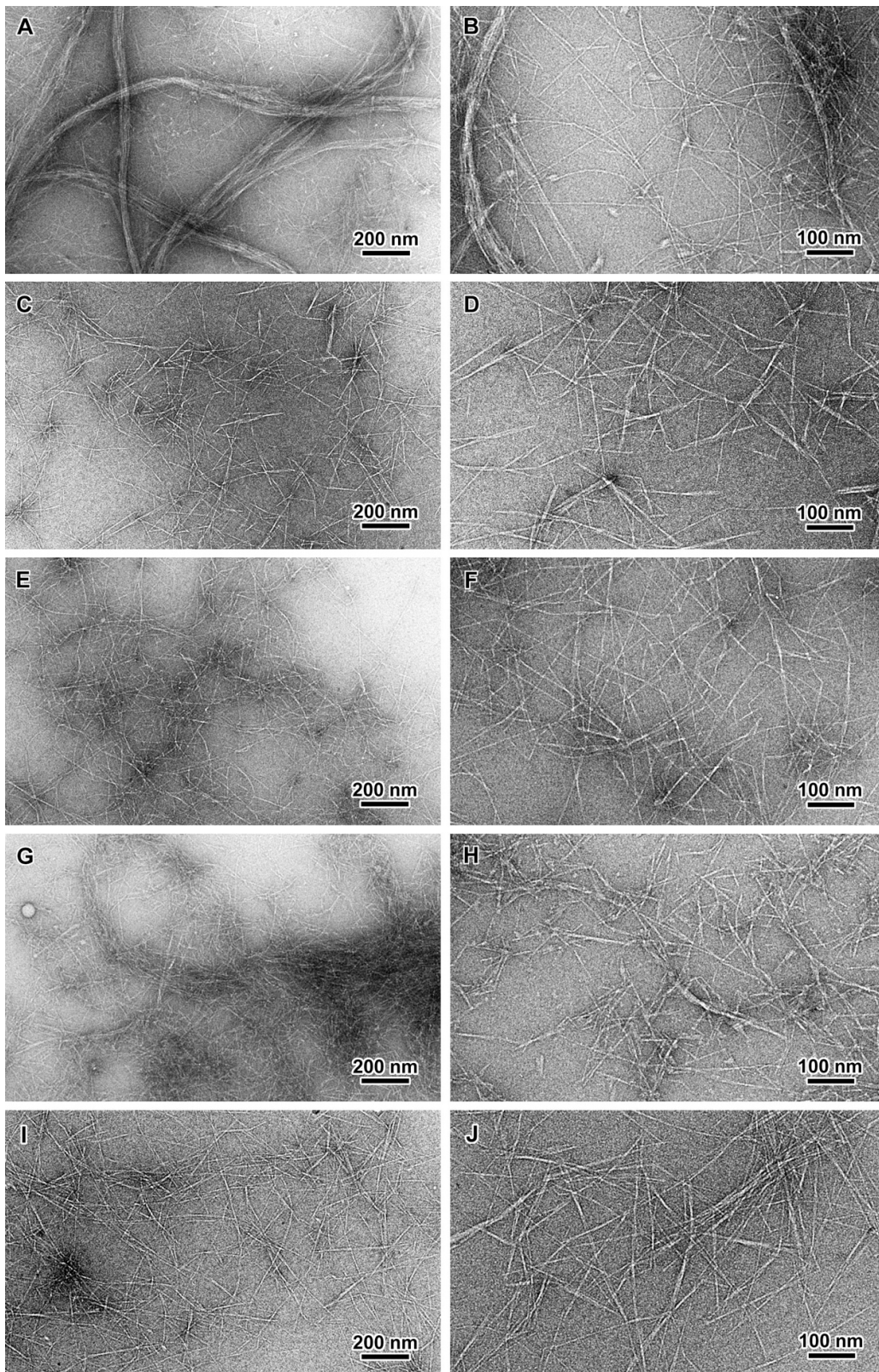


Figure 1. TEM images of negatively stained preparations from Bas-800 (A,B), Bas-1000 (C,D), Bas-1300 (E,F), Carb-800 (G,H) and Neut-800 (I,J).

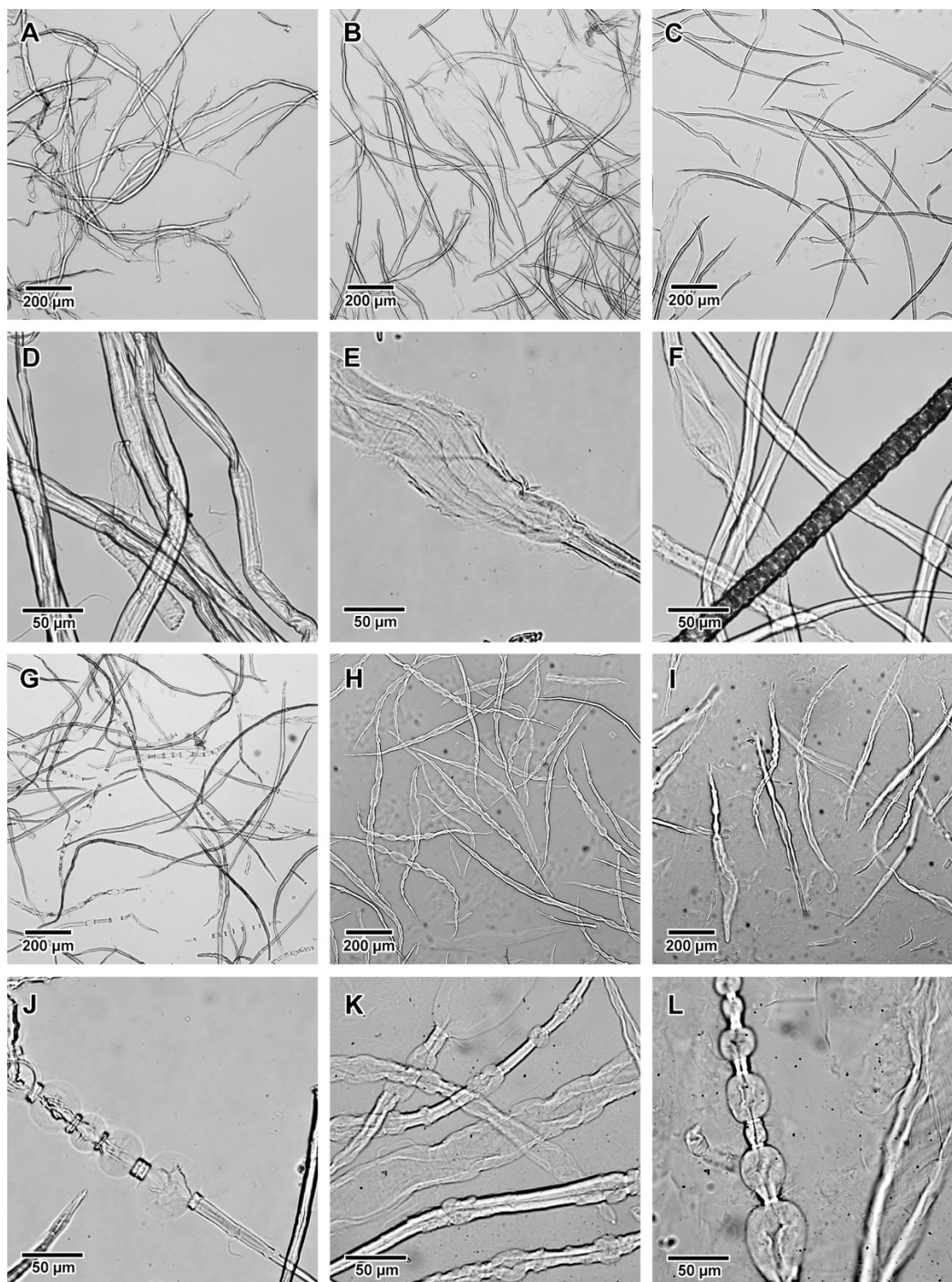


Figure 2. Optical micrographs of virgin fibers (A,D), Neut-800 (B,E), Bas-800 (C,F), Carb-800 (G,J), Bas-1000 (H,K), and Bas-1300 (I,L) treated fibers.

Oxidized fibers with a carboxyl content around $700\text{-}800\ \mu\text{mol.g}^{-1}$ exhibit a heterogeneous morphology. Swollen fibers with loose cell walls can be seen next to long fibers without any visible change in their aspect. In carboxymethylated fibers Carb-800, some of the fibers exhibit balloon-like swollen regions. This phenomenon was commonly observed during dissolution of cellulose fibers in N-methylmorpholine-N-oxide / water mixtures (Cuissinat & Navard 2007), or

cellulose fibers swollen by alkali and carbon bisulfate (Ott, Spurlin & Grafflin 1954). This morphology was explained by the radial expansion of the cellulose in the secondary wall causing the primary wall to burst. However, the swelling was not homogeneous and unswollen sections remain, restricting the uniform expansion of the fiber and promoting the formation of balloons. With increasing carboxyl content, the fraction of swollen fibers increased. In oxidized fibers with a carboxyl content over $1000 \mu\text{mol.g}^{-1}$ (Bas-1000 and Bas-1300), most fibers were swollen and many of them showed a balloon structure (**Figure 1H,K and 1I,L**). The heterogeneous morphology in oxidized or carboxymethylated fibers might be due to a difference in the accessibility of cellulose fibers to chemical reagents (NaClO for oxidation and sodium chloroacetic acid for carboxymethylation). We infer that the successful defibrillation of chemically-treated fibers by extrusion is favored by the swelling of fibers, thus facilitating the breakdown of cell walls and the individualization of the cellulose nanofibrils. The fiber expansion also increases its flexibility and reduces the risk of clogging by accumulation of compressed fibers at the extremity of the screw. This might explain the easier extrusion of oxidized or carboxylated cellulose fibers as their carboxyl content exceeded a critical threshold. The expansion of fibers after oxidation or carboxymethylation is further highlighted from WRV measurement. The WRV of neat NDP was 52% and markedly grew after oxidation treatment, reaching about 323% and 490% for Bas-800 and Bas-1300 treated fibers respectively (**Table 1**). The WRV also increased with increasing carboxyl content, confirming the tendency of the notable expansion of the fibers revealed by optical microscopy observation (**Figure 2**).

The mechanical properties of CNF films prepared by drying CNF suspensions and storage at 50% R.H. were evaluated by tensile tests. Typical stress–strain curves for CNF nanopaper and fiber films prepared by casting and drying at 40°C are shown in **Figure 3A** from which the tensile strength, tensile modulus, and strain at break were collected and given in **Table 1**. For comparison purpose, the mechanical properties of films from pretreated and neat fibers were included (Neat fibers, Pap-800) and their tensile curve added in **Figure 3A**. For CNF films, the tensile curve shows an elastic region with a limit deformation up to about 1 % followed by a strain-hardening plastic region extending from 1 to 2-4 %.

The strength of film from neat (Neat fiber) and pretreated fibers with carboxyl content 800 (Pap-800) was quite low, around 3.6 and 14.5 MPa, respectively. The enhancement observed after the oxidation treatment is presumably due to improved bonding between fibers as a result from the carboxylic groups generated and hydration of the cellulose fibers that improve the contact between cellulose fibers. After TSE and for samples with carboxyl content exceeding $700 \mu\text{mol.g}^{-1}$, a strong enhancement of the tensile modulus and strength is observed which is

explained by the formation of CNFs generating entangled network held through hydrogen bonding and to form homogenous and compact structure (Henriksson et al. 2008). For films of fibers oxidized under basic condition, the tensile strength at carboxyl content of 750, 1000 and 1350 reached 42, 48 and 52 MPa and the tensile modulus was 2.8, 5.6 and 6.8 GPa, respectively.

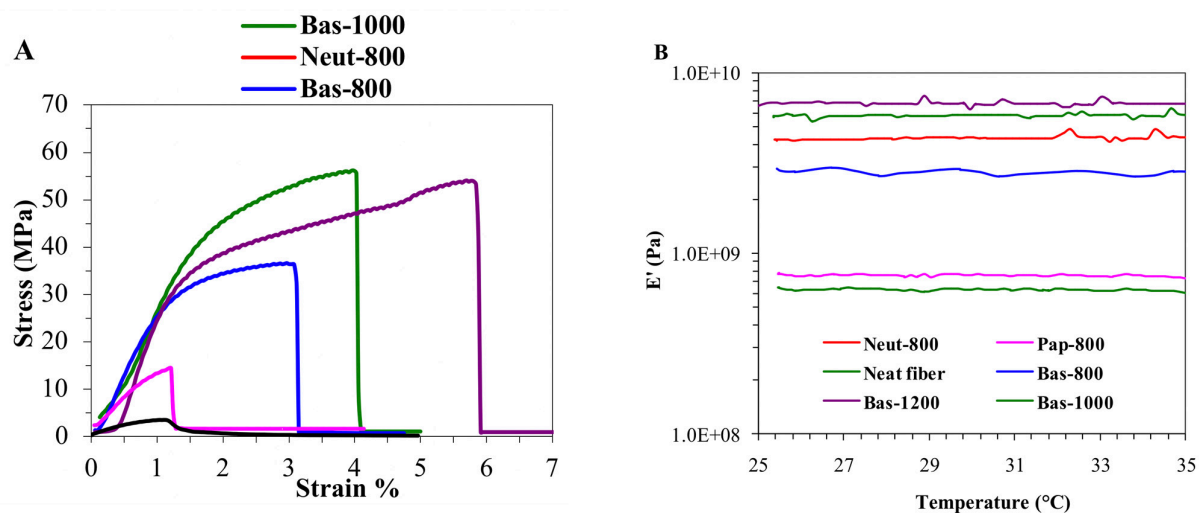


Figure 3. (A) Typical stress-strain curves for cellulose films and (B) storage modulus (E') vs. temperature of cellulose films prepared from extruded fibers. Pap-800: film from basic oxidized fibers with a carboxyl content of $800 \mu\text{mol.g}^{-1}$ without extrusion.

This steady increase in mechanical performance of extruded films could be explained by the increase in the nanosized fraction of cellulose fibrils, which is responsible for the strong reinforcing effect of extruded cellulose films. Given their nanoscale, flexibility resulting from the coexistence of disorganized and crystalline domains within the cellulose fibrils, CNFs are known to form tightly interconnected networks held by a strong hydrogen-bonding between neighboring CNFs. This led to a dense nanopaper structure with a low porosity and high capacity to transfer stress from fibril-to-fibril (Henriksson et al. 2008, Isogai, Saito & Fukuzumi 2011). Moreover, albeit their similar carboxyl content, the strength and tensile modulus of nanopaper of Neut-800 were higher than that of Bas-800. Two reasons might account for the disparity in the mechanical performance of the CNF film: (i) the higher nanosized CNF fraction from Neut-800 in comparison of Bas-800, and (ii) the presence of large bundles of fibrils from Bas-800 that were not observed in CNFs from Neut-800, suggesting a poor fibrillation efficiency in Bas-800 fibers.

However, referring to literature data, it worth to note that the strength of the films from CNFs produced by TSE was lower in comparison with those from CNFs produced by HPH (Fujisawa et al. 2011) even though the same method of preparation of the CNF film was adopted (i.e. casting-drying without pressing) and TEMPO-mediated oxidized fibers was used. Strength

within the range of 120 to 150 MPa was reported along with a tensile modulus between 7 to 12 GPa (Henriksson et al. 2008). One possible reason justifying this difference is the lower fibrillation efficiency of TSE compared to HPH and the difference in the morphology of the cellulose fibrils produced from the two methods. The later led to better individualization of the cellulose nanofibrils attaining the level of the elementary fibrils with diameter around 3-5 nm, especially when a chemical pretreatment was adopted (Besbes, Alila & Boufi 2011).

DMA was also performed on cellulose films to evaluate the tensile modulus (E') of films within the linear domain with good accuracy (**Figure 3B**). For all tested films, E' remained nearly constant in the temperature domain 20-60°C with a magnitude depending on the carboxyl content. A strong increase in E' by about one order of magnitude was noted for films produced from extruded fibers. The magnitude of E' increased with increasing carboxyl content of extruded fibers, indicating an enhancement in the stiffness of the nanopaper. This effect is in line with tensile test data and is presumably due to the increase in the fraction of nanofibrils.

The morphology of the different cellulose films produced from extruded and pretreated fibers was studied by FE-SEM observation of surface and cross-section fracture of films (**Figure 4**). At low magnification, micron-sized cellulose fibers dispersed within a web-like tight network can be seen which corresponds to the fraction of intact and partially fibrillated fibers. At high magnification, a random-in-plane web-like network structure formed by entangled CNFs tightly bound to each other can be seen. This interconnected network structure with a low porosity in the range 10-30 nm accounts for the high density of CNF films and their higher strength and stiffness compared to films from non-extruded fibers. The width of CNFs ranges from 10 to 30 nm which is higher than that revealed by TEM. A possible reason is the aggregation of individual cellulose nanofibrils during the drying process.

The cross-section of the CNF films (**Figure 5**) reveals a layered structure which is the typical structure observed in nanopapers from CNFs produced by high pressure homogenization or microfluidization (Henriksson et al. 2008). This layered structure has been ascribed to the deposition of successive layers of CNFs during filtration. However, this explanation cannot be presently supported considering the mode of preparation of CNF film based on a simple evaporation of a 0.2 wt% CNF suspension in a Petri dish. The hypothesis of a concentration-induced aggregation and floc formation at a later stage of water removal has been also suggested to explain this organization (Benítez et al. 2013).

The chemical pretreatment of cellulose fibers and their mechanical disintegration can affect the crystalline degree of the material leading to decrease in the reinforcing potential of CNFs. The effect of the chemical treatments and extrusion on the crystallinity of the different samples

was analyzed by X-ray diffraction (**Fig. 6**). All diffraction patterns show reflections of cellulose I at $2\theta = 16.2, 22.4$ and 34.6° associated to $(1\bar{1}0)/(110)$, (200) and (004) crystal planes, respectively ([French 2014](#))

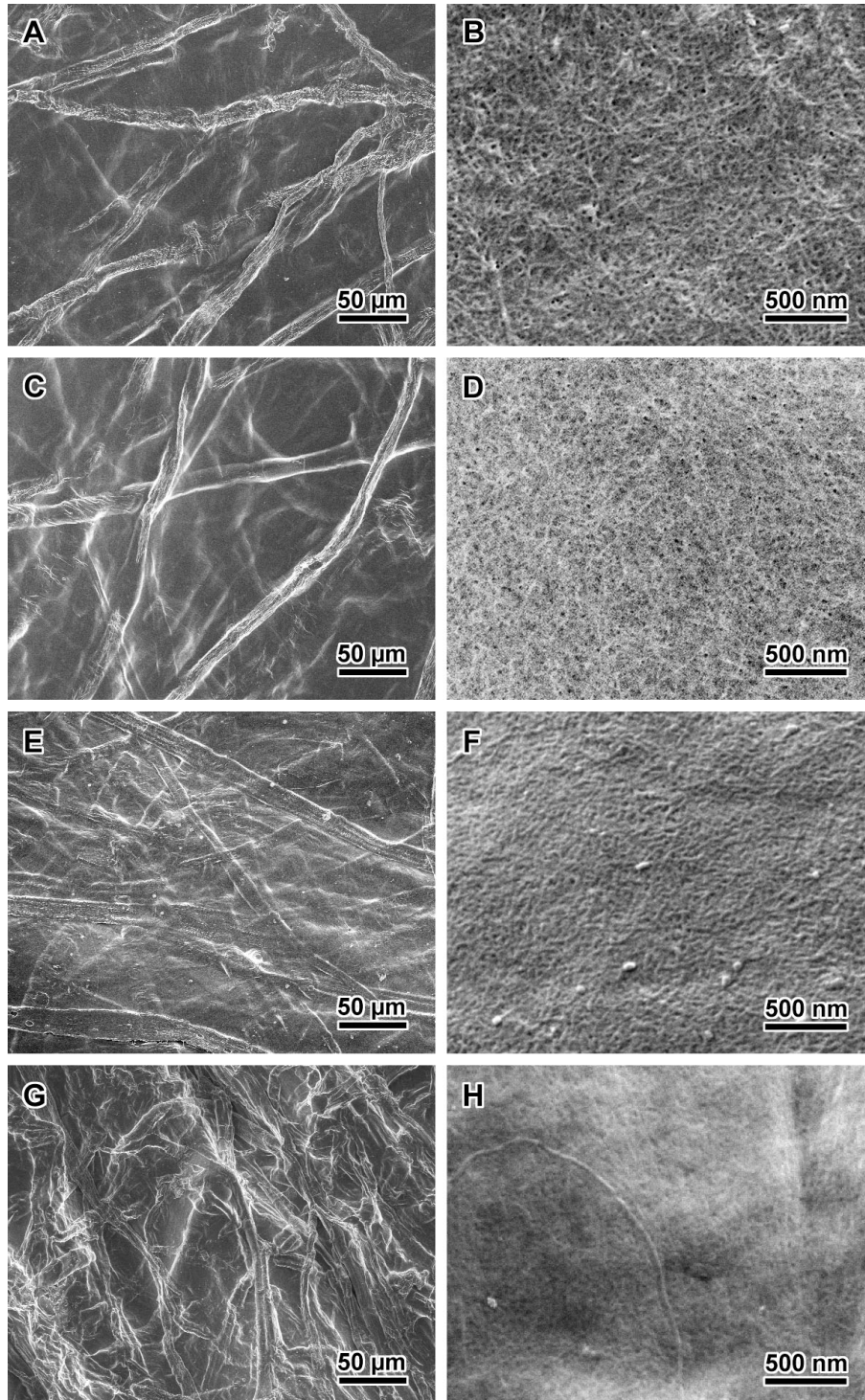


Figure 4. FE-SEM images of CNF films from extruded treated fibers: A,B) Bas-800; C,D) Bas-1300; E,F) Neut-800; G,H) Carb-800.

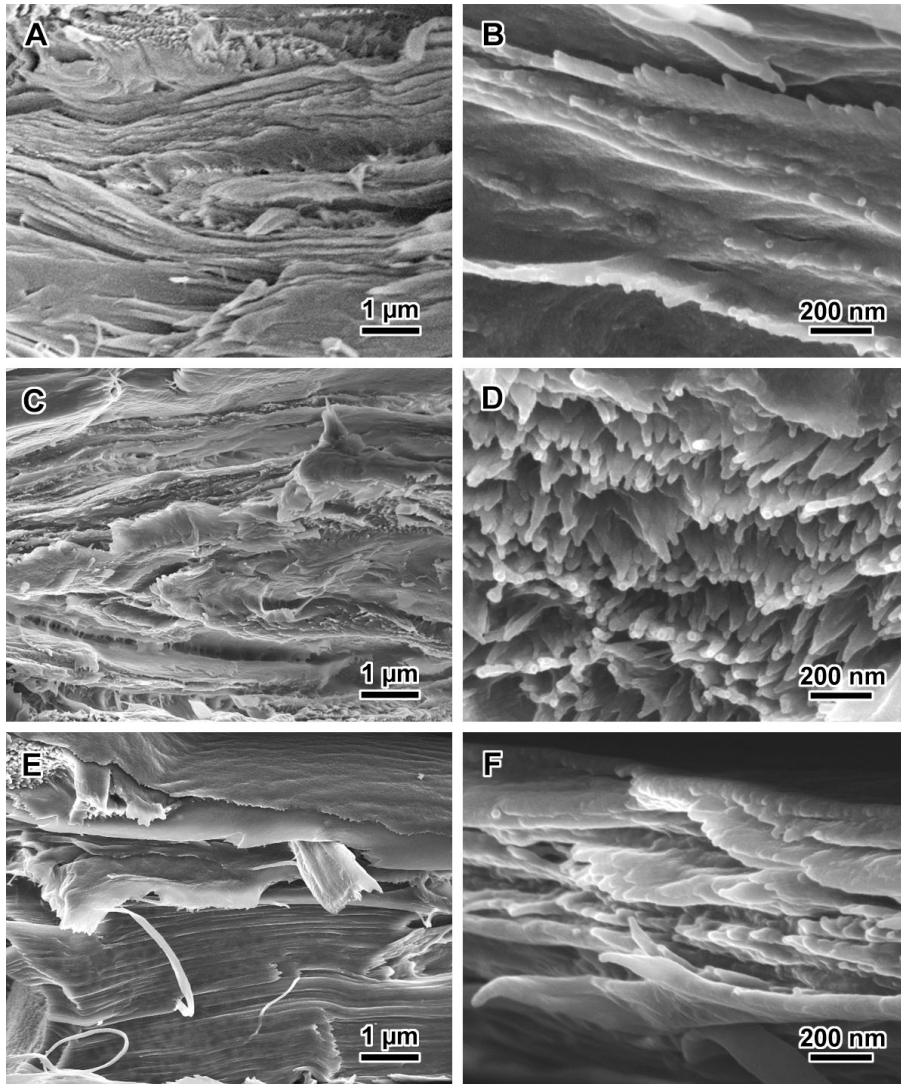


Figure 5. FE-SEM images of cross-sections of freeze-fractured CNF films from extruded treated fibers: A,B) Bas-800; C,D) Bas-1300; E,F) Neut-800.

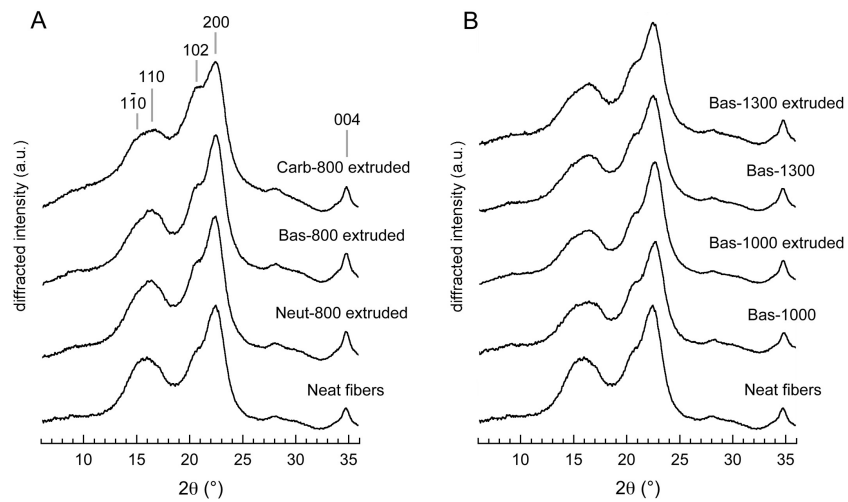


Figure 6. X-ray diffraction profiles for neat, oxidized and carboxylated fibers before and after extrusion.

For oxidized fibers, the CrI remained within the 0.74-0.77 range over a carboxyl content between 800 and 1300 $\mu\text{mol.g}^{-1}$ and did not change after the extrusion of treated fibers, implying that the crystalline structure was not significantly affected neither by the oxidation treatment nor by the extrusion process. However, in carboxymethylated fibers, the CrI for sample with a carboxyl content around 800 decreased to 0.57 indicating a decrease in the crystallinity of cellulose fibers after the carboxymethylation. This phenomenon has already been reported in the literature and explained by the breakage of hydrogen bonds in the crystalline regions of cellulose chains during the carboxymethylation reaction (Eyholzer et al. 2010).

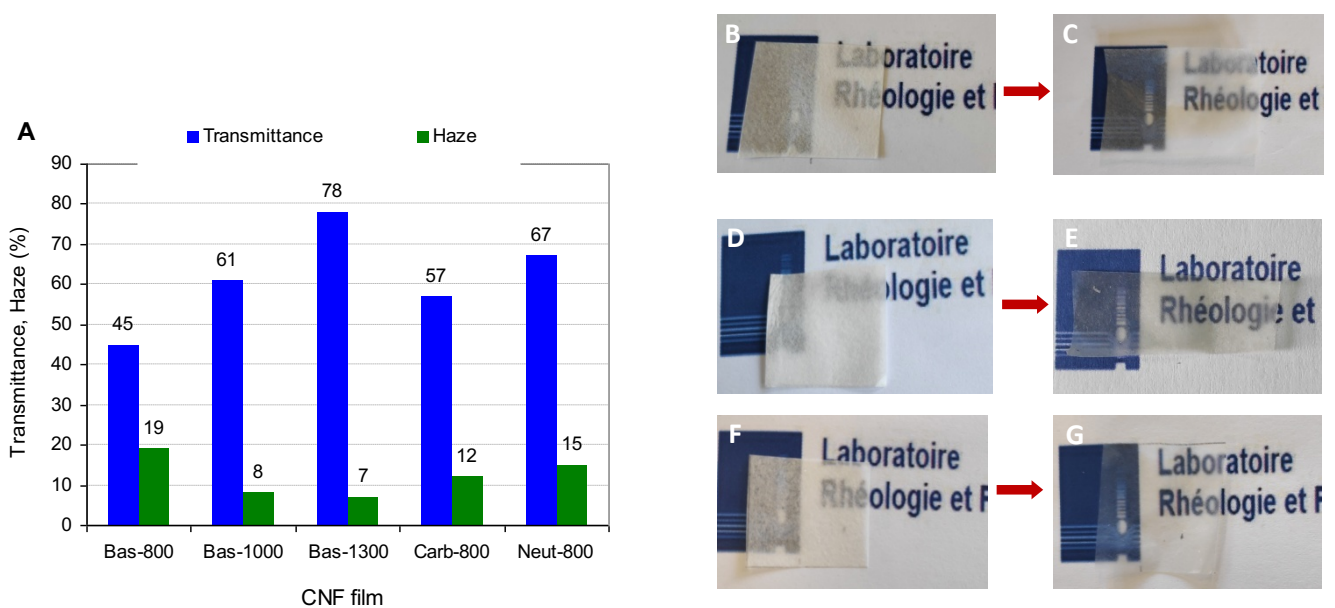


Figure 7. (A) Transmittance and haze at 600 nm of CNF films produced by extrusion of pretreated fibers at different carboxyl content. Visual appearance of film Bas-800 (B) before and (C) after extrusion; Bas-1000 before (D) and after (E) extrusion of fibers; Bas-1300 before (F) and after (G) extrusion of fibers.

The transparency degree of thin films produced from cellulose fibers or nanofibers without any additive or pigment depends on a number of parameters including thickness, fiber or fibril width, porosity and surface roughness. Due to the mismatch between the refractive index of air ($n=1$) and cellulose ($n=1.5$) light is scattered at the fibril/air interface during propagation through the film, which results in the reduction of transmitted light and consequently in the transparency of the film. The scattering intensity strongly depends on the particle size and wavelength and, below a critical size of about 40 nm, the material turned transparent to light without any scattering effect. The transmittance and haze at 600 nm are shown in **Figure 7**. Haze is a measurement of the light scattering characteristics of a material and is responsible for

the difficulty to clearly see objects through a film. The light transmittance for all CNF films from extruded fibers with thickness around 30 μm is above 45 % (at 600 nm) with a haze being lower than 20 which is indicative of that a high fraction of incident light can cross over the film without being scattered. At a higher carboxyl content, the transmittance further increased up to 80 % at a 1300 $\mu\text{mol.g}^{-1}$ carboxyl content and with a haze around 7. The drop in haze corresponds to a decrease in scattered light which is due to the lower porosity, enhancement in the nanosized fraction and reduction in surface roughness of CNF films. This result agrees with literature data concerning the correlation between transparency/haze of nanopaper films and the CNF morphology (Hsieh, Koga, Suganuma, & Nogi 2017, Zhu et al. 2013). The visual appearance of CNF films supported the transmittance measurement, where it can clearly be seen that cellulose film from oxidized non-extruded fibers looks white and rather opaque and turned to translucent-transparent films when the film was produced from extruded fibers.

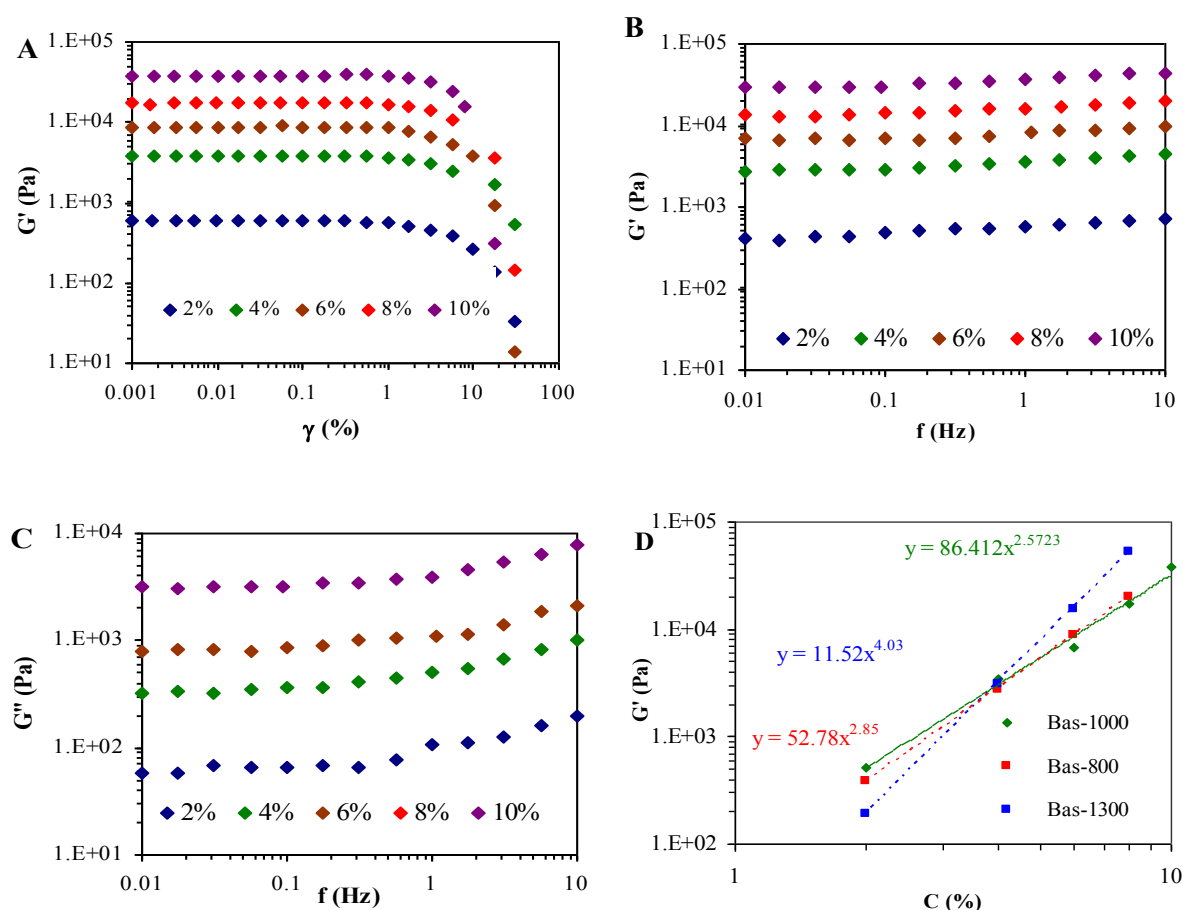


Figure 8: (A) Storage modulus G' vs. strain amplitude, (B) storage modulus G' and (C) loss modulus G'' vs. frequency for Bas-1000 CNFs, and (D) storage modulus G' at 1 Hz vs. solid content C . The lines correspond to the fits of the power law $G'=KC^n$ on experimental measurements.

The rheological behavior of the CNF suspension at different solid contents was investigated by oscillatory sweep measurements of the storage modulus (G') and loss modulus (G'') as a function of strain amplitude (γ) or frequency (f). Examples of oscillatory sweep measurements for Bas-1000 CNF gel are given in **Figure 8A-C**. For all CNF suspensions, a transition from a linear to nonlinear viscoelastic behavior was observed over a critical strain γ_c in the range of 2–4% with an abrupt drop of the magnitude of G' which is the result of the breakdown of the CNF network under the effect of deformation. In addition, all of the CNF suspensions produced by TSE exhibited a gel-like character over a solid content in the range of 1 to 10 %, as attested by the dominance of G' over G'' in the measured frequency range with (G' being about one decade higher than G'' over the whole frequencies domain). For all studied samples and with the solid content ranging from 2 to 10 %, both G' and G'' were nearly independent of frequency and carboxyl content as seen in Figure S4. This property is consistent with the gel-like behavior typically observed for CNFs produced by other disintegration methods such as high-pressure homogenization or grinding (Nechyporchuk, Belgacem, & Pignon 2014). The origin of this effect was explained by the tendency of CNF to form an interconnected three-dimensional network, even at low concentration ($C < 0.5\%$) thanks to the flexibility of the cellulose nanofibrils along with their high aspect ratio (Pääkkö et al. 2007, Nechyporchuk, Belgacem & Pignon 2016). The upholding of the gel character of all the CNFs produced by TSE in the domain of solid content between 1 to 10 %, regardless of the carboxyl content and the fibrillation extent, suggested that the rheological properties of the CNFs were dominated by the presence of nanosized fibrils.

A decrease in the magnitude of G' as the solid content C is getting down is observed, which is expected due to the weakening of the network resulting from the decrease in the number of fibril–fibril contact upon dilution of the CNF gel. A power-law dependence of G' with CNF concentration ($G' = KC^n$) in the linear domain was noted for the different gel, where C is the weight concentration of CNFs and the K factor and n power are characteristic of the individual nanofibril characteristics and the structural property of the CNF suspension, respectively. The fit of the power laws is shown in **Figure 8D** for basic oxidation. The K factor attained about 52, 86 and 11 Pa for Bas-800, Bas-1000 and Bas-1300 respectively, while the n power index is about 2.87, 2.57 and 4.03, for Bas-800, Bas-1000 and Bas-1300, respectively. The regression coefficients R^2 are higher than 0.99. Based on theoretical consideration, the value of n in the power-law relation between G vs. solid content of polymer gel should be 2–2.5 (MacKintosh, Kää & Janmey 1995). However, referring to literature data, the wide range of the n values from 1 to 5 has been reported without soundly clarifying the origin of this variation (Nechyporchuk,

Belgacem & Pignon 2016). A similar power-law behavior was also reported for carbon nanotube suspension with n varying from 2 to 7 depending on the aspect ratio and surface treatment. The highest value was observed for nanotubes with the shortest length while for the long fibrils the n value is close to 2-2.5 (Rahatekar et al. 2009). Recently, a rheological investigation on chitin nanofibrils with different lengths and degrees of aggregation has shown a strong dependence of the n value on their aspect ratio, degree of dispersion and self-interaction (Yokoi, Tanaka, Saito & Isogai 2017). The n value was found to increase from 2.7 to 3.8–3.9 as nanofibrils self-organized from a randomly oriented structure into a nematic ordered arrangement. One possible reason explaining the higher value of n power in for Bas-1300 is the lower length of these CNFs in comparison with CNFs from Bas-800 and Bas-1000. The decrease in CNF length would result from secondary reaction, mostly β -elimination, accompanying the oxidation reaction under basic condition inducing cellulose chains breaking (Shinoda, Saito, Okita & Isogai 2012). The decrease in the nanofibril length at high carboxyl content in TEMPO-mediated oxidation of cellulose was also reported by Isogai et al. (Isogai, Saito & Fukuzumi 2011) where a correlation between the carboxyl content, the length and the degree of polymerization (DP) was established (Shinoda, Saito, Okita & Isogai 2012). The AFM observation of CNFs from Bas-800, Bas-1000 and Bas-1300 supported also the hypothesis of a decrease in the CNF length as their carboxyl content is increasing (**Figure S2A-C**). However, the contribution of the carboxyl content should not be disregarded. In fact, with the increase in carboxyl content, the CNFs became more surface-charged and less inclined to interact with neighboring CNFs due to the electrostatic repulsion effect. The contribution of this effect is probably more marked at low CNF concentration, which might explain the lower magnitude of G' for Bas-1300 at a solid content lower than 3 wt%. At higher concentration, the morphology of CNFs, especially their length, will prevail over the other effects. This could explain the difference observed in **Figure 8D**.

The steady-state viscosities as a function of the shear rate for CNF suspensions displayed a typical shear-thinning behavior of CNF gel which is attributed to the disentanglement and alignment of CNFs along the shear direction under the low shear force, causing a gradual decrease in viscosity, which agrees with literature data (Nechyporchuk, Belgacem & Pignon 2016). An example of the steady flow curves for Bas-1000 CNFs at different solid contents is given in **Figure S5**.

4. Conclusion

Commercial never-dried cellulose pulp was used as starting material to produce CNF gels at high consistency (10wt% solid content) by TSE. Three approaches of chemical pretreatment consisting in a TEMPO-mediated oxidation at basic and neutral condition and carboxymethylation with sodium chloroacetic acid were adopted to generate carboxyl groups at controlled amount. Without any chemical pretreatment, it was impossible to extrude NDP because of the clogging of fibers impeding recirculation for multiple passes. The successful disintegration of cellulose fibers into CNF gels was observed only for samples with a carboxyl content exceeding $700 \mu\text{mol.g}^{-1}$, irrespective of the method of chemical pretreatment. Based on optical observation, it was proposed that the chemical pretreatment led to a swelling of the fibers turning them more flexible to be recirculated through TSE without any risk of clogging. The swelling of fibers facilitates also their breakdown by reducing the interfibrillar interaction through hydrogen bonding.

The increase in carboxyl content led to an increase in the nanosized fraction and enhancement in the tensile modulus and strength of nanopaper from CNF gels. FE-SEM observation of CNF films revealed a random-in-plane web-like network structure, exhibiting a layered structure when cross-section observed.

The successful disintegration of commercial eucalyptus pulp into cellulose nanofibrils by TSE at a solid content of 10% contributed to further develop this relatively new processing method to produce CNFs. This work has contributed to identify some of the parameters controlling the breakdown of cellulose fibers into nanoscale objects when a chemical pretreatment based on TEMPO-mediated oxidation or carboxymethylation. Although this chemical pretreatment was necessary to run the process, the high solid content of the produced CNFs without any risk of clogging and the use of conventional commercial TSE constitutes the main advantage of this processing route. The lower energy consumption of TSE is another merit of this method. Work is under progress to scale up the production of CNFs via TSE using oxidized fibers with carboxyl content around $1000 \mu\text{mol.g}^{-1}$ and using a pilot twin-screw extruder.

Acknowledgement

This work has been partially supported by LabEx Tec 21 (Investissements d'Avenir – grant agreement #ANR-11-LABX-0030). LRP and CERMAV are part of Institut Carnot PolyNat (Investissements d'Avenir – grant agreement #ANR-11-CARN-030-01). This work was developed in the framework of Glyco@Alps, supported by the French National Research

Agency under the "Investissements d'Avenir" program (ANR-15-IDEX-02). The authors thank the NanoBio-ICMG Platform (FR 2607, Grenoble) for granting access to the Electron Microscopy facility. The FE-SEM images were recorded at the CMTC characterization platform of Grenoble INP supported by LabEx CEMAM (Investissements d'Avenir, grant agreement #ANR-10-LABX-44-01). We thank Rachel Martin (CMTC) for the FE-SEM observations. The PHC-Utique program (19G1123) is also acknowledged.

References

- Baati, R. Mabrouk, A.B., Magnin, A., & Boufi, S. (2018) CNFs from twin screw extrusion and high pressure homogenization: A comparative study, *Carbohydrate Polymers*, 195, 321–328.
- Baati, R., Magnin, A., & Boufi, S. (2017) High solid content production of nanofibrillar cellulose via continuous extrusion. *ACS Sustainable Chemistry & Engineering*, 5(3), 2350–2359.
- Benhamou, K., Dufresne, A., Magnin, A., Mortha, G., & Kaddami, H. (2014) Control of size and viscoelastic properties of nanofibrillated cellulose from palm tree by varying the TEMPO-mediated oxidation. *Carbohydrate Polymers*, 99, 74–83.
- Benítez, A.J., Torres-Rendon, J., Poutanen, M., Walther, A. (2013) Humidity and multiscale structure govern mechanical properties and deformation modes in films of native cellulose nanofibrils, *Biomacromolecules*, 14, 4497–4506.
- Besbes, I., Alila, S., & Boufi, S. (2011) Nanofibrillated cellulose from TEMPO-oxidized eucalyptus fibres: Effect of the carboxyl content. *Carbohydrate Polymers*, 84, 975–983.
- Boufi, S., González, I., Delgado-Aguilar, M., Quim, T. & Mutjé, P. (2016) Nanofibrillar cellulose as additive in papermaking process: A review. *Carbohydrate Polymers*, 154, 151–166.
- Cuissinat, C., & Navard, P. (2006) Swelling and dissolution of cellulose, Part I: free floating cotton and wood fibres in N-methylmorpholine-N-oxide–water mixtures. *Macromolecular Symposia* 244, 1–18.
- Eyholzer, C., Bordeanu, N., Lopez-Suevos, F., Rentsch, D., Zimmermann, T., & Oksman, K. (2010) Preparation and characterization of water-redispersible nanofibrillated cellulose in powder form. *Cellulose*, 17, 19–30.
- French, A.D. (2014) Idealized powder diffraction patterns for cellulose polymorphs. *Cellulose* 21, 885–896.
- Fujisawa, S., Okita, Y., Fukuzumi, H., Saito, T., & Isogai, A. (2011) Preparation and characterization of TEMPO-oxidized cellulose nanofibril films with free carboxyl groups, *Carbohydrate Polymers*, 84, 579–583.
- Henriksson, M., Berglund, L.A., Isaksson, P., Lindström, T., & Nishino, T. (2008) Cellulose nanopaper structures of high toughness, *Biomacromolecules*, 9, 1579–1585.
- Ho, T.T.T., Abe, K., Zimmermann, T., & Yano, H. (2015) Nanofibrillation of pulp fibers by twin-screw extrusion. *Cellulose*, 22, 421–433.
- Hsieh, M.C., Koga, H., Suganuma, K., & Nogi, M. (2017) Hazy transparent cellulose nanopaper, *Scientific Reports*, 7, 41590.
- Isogai, A., Saito, T., & Fukuzumi, H. (2001) TEMPO-oxidized cellulose nanofibers. *Nanoscale* 3, 71–85.
- Lavoine, N., Desloges, I., Dufresne, A., & Bras, J. (2012) Microfibrillated cellulose – its barrier properties and applications in cellulosic materials: a review. *Carbohydrate Polymers*, 90, 735–764.
- MacKintosh, F. C., Kää, J., & Janmey, P. A. (1995) Elasticity of semiflexible biopolymer networks, *Physical Review Letters*, 75, 4425–4428.
- Nechyporchuk, O. Belgacem, M.N. & Pignon, F. (2016) Current progress in rheology of cellulose nanofibril suspensions. *Biomacromolecules*, 17, 2311–2320.

- Nechyporchuk, O., Belgacem, M. N., & Pignon, F. (2014) Rheological properties of micro-/nanofibrillated cellulose suspensions: wall-slip and shear banding phenomena. *Carbohydrate Polymers*, *112*, 432–439.
- Ott, E., Spurlin, H.M., & Grafflin, M.W. Cellulose and Cellulose Derivatives (Part 1), Interscience Publisher, New York, 1954.
- Pääkkö, M., Ankerfors, M., Kosonen, H., Nykänen, A., Ahola, S., & Österberg, M. (2007) Enzymatic hydrolysis combined with mechanical shearing and high pressure homogenization for nanoscale cellulose fibrils and strong gels. *Biomacromolecules*, *8*(6), 1934–1941.
- Rahatekar, S.S., Koziol, K.K., Kline, S.R., Hobbie, E.K., Gilman, J.W., & Windle, A.H. (2009) Length-dependent mechanics of carbon nanotube networks. *Advanced Materials*, *20*(1), 874–878.
- Rezayati-Charani, P., Dehghani-Firouzabadi, M., Afra, E., & Shakeri, A. (2013) Rheological characterization of high concentrated MFC gel from kenaf unbleached pulp. *Cellulose*, *20*, 727–740.
- Rol, F., Belgacem, N., Meyer, V., Petit-Conil, M., & Bras, J. (2019) Production of fire-retardant phosphorylated cellulose fibrils by twin-screw extrusion with low energy consumption, *Cellulose*, *26*, 5635–5651.
- Rol, F., Karakashov, B., Nechyporchuk, O., Terrien, M., Meyer, V., Dufresne, A., Belgacem, M. N., & Bras, J. (2017) Pilot scale twin screw extrusion and chemical pretreatment as an energy efficient method for the production of nanofibrillated cellulose at high solid content, *ACS Sustainable Chemistry and Engineering*, *5*, 6524–6531.
- Rol, F., Saini, S., Meyer, V., Petit-Conil, M., & Bras, J. (2019) Production of cationic nanofibrils of cellulose by twin-screw extrusion, *Industrial Crops and Products*, *137*, 81–88.
- Saito, T., Kimura, S., Nishiyama, Y., & Isogai, A. (2007) Cellulose nanofibers prepared by TEMPO-mediated oxidation of native cellulose. *Biomacromolecules*, *8*, 2485–2491.
- Segal, L., Creely, J.J., Martin, A.E. Jr, & Conrad, C.M. (1959) An empirical method for estimating the degree of crystallinity of native cellulose using the X-ray diffractometer. *Textile Research Journal*, *29*, 786–794.
- Shinoda, R., Saito, T., Okita Y., & Isogai, A. (2012) Relationship between length and degree of polymerization of TEMPO-oxidized cellulose nanofibrils. *Biomacromolecules*, *13*, 842–849.
- Yokoi, M., Tanaka, R., Saito, T. & Isogai, A. (2017) Dynamic Viscoelastic functions of liquid-crystalline chitin nanofibril dispersions. *Biomacromolecules*, *18*, 2564–2570.
- Zhu, H., Parvinian, S., Preston, C., Vaaland, O., Ruan, Z., & Hu, L. (2013) Transparent nanopaper with tailored optical properties. *Nanoscale*, *5*, 3787–3792.

Supporting Information

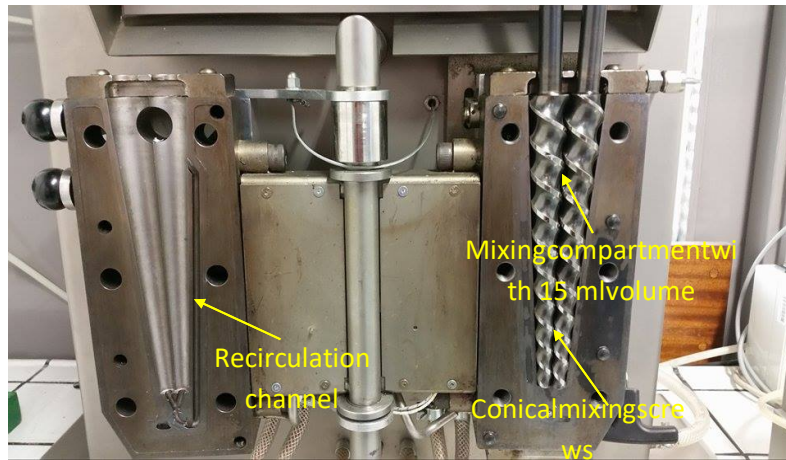


Figure S1: The twin-screw mini extruder used for the disintegration of fibers.

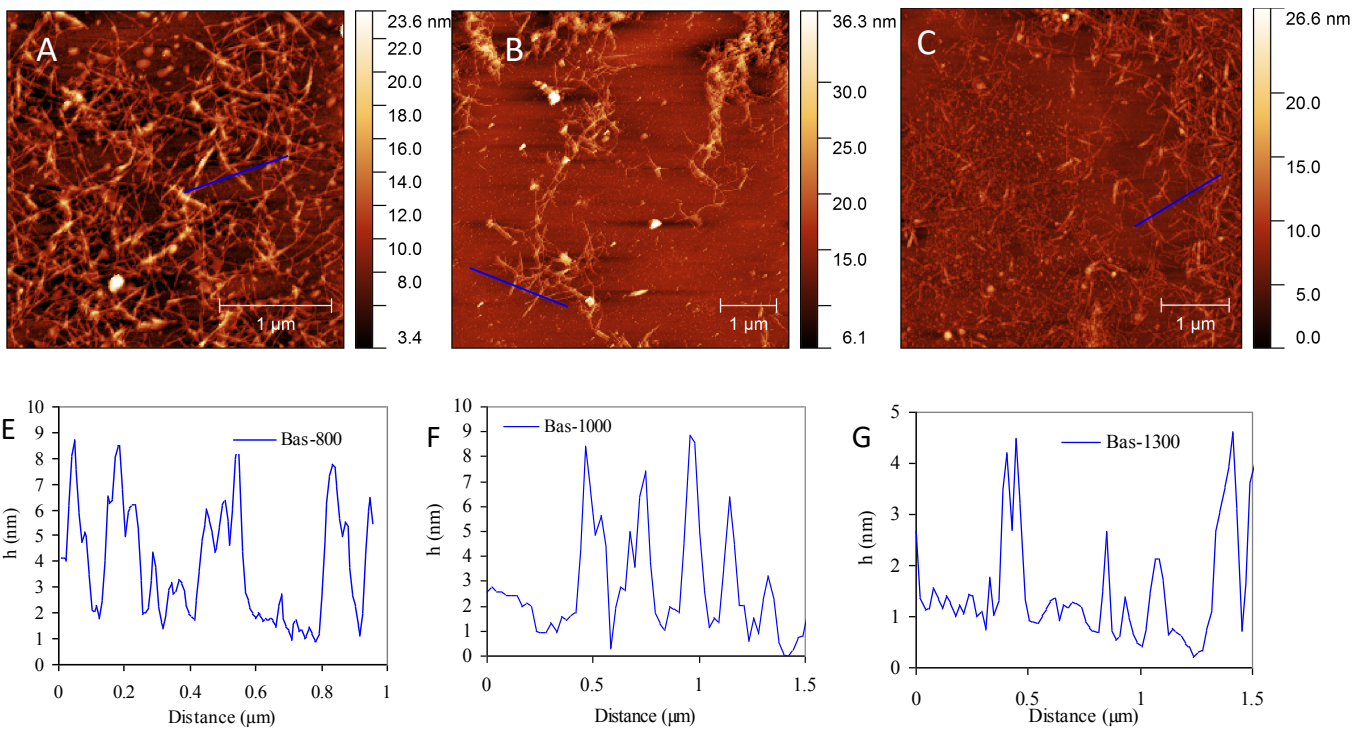
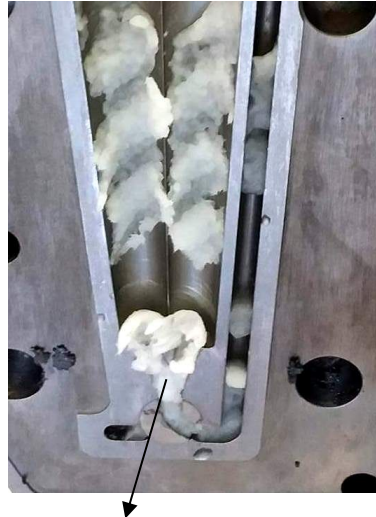


Figure S2: AFM height images of CNFs produced by TSE from (A) Bas-800, (B) Bas-1000, (C) Bas-1300, (D) and the corresponding cross section profile analysis corresponding to the blue arrow (E) Bas-800, (F) Bas-1000, (G) Bas-1300.



The fibers stack at the extremity of the screw, forming a plug that prevents the material from recirculating through the channel

Figure S3: photos showing how fibers were stacked at the extremity of the screw when neat pulp or oxidized fibers with carboxyl content lower than $600 \mu\text{mol.g}^{-1}$ were used for extrusion.

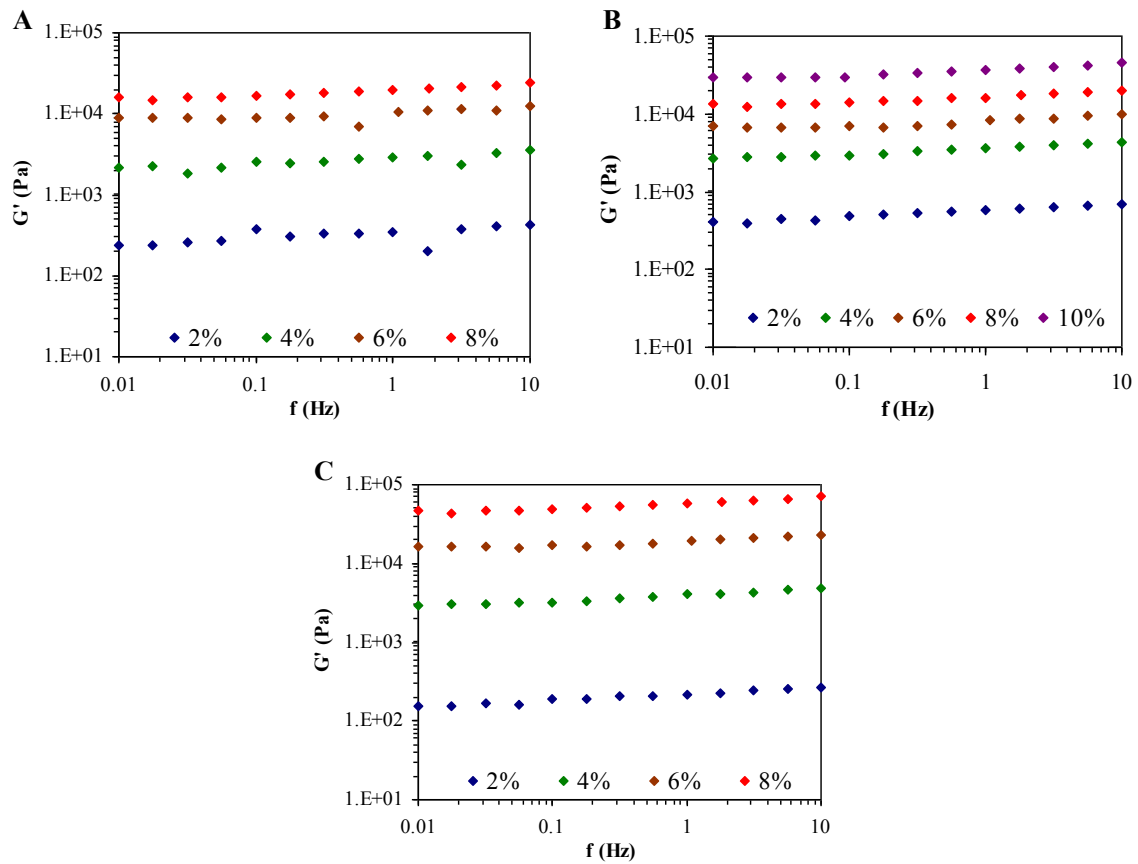


Figure S4: Storage modulus G' vs. frequency for (A) Bas-800, (B) Bas-1000 and (C) Bas-1300 CNFs at different solid contents.

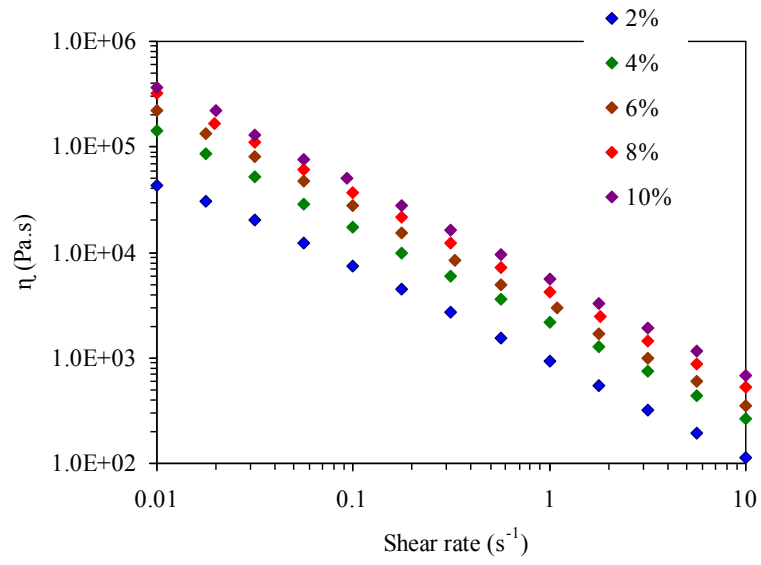


Figure S5: Steady-state viscosity vs. shear rate of a CNF gel from Bas-1000.